

Three-Dimensional Inverse Scattering Applied to Cross-Well Induction Sensors

Aria Abubakar and Peter M. van den Berg

Abstract—Cross-well induction logging as known in the oil industry is a method for determining the electrical conductivity distribution between boreholes from the low-frequency electromagnetic field measurements in the boreholes. In this paper, we discuss the reconstructions of the three-dimensional (3-D) conductivity distribution using the contrast source inversion (CSI) method. In order to improve the reconstruction results, the concept of the extended Born approximation has been used to arrive at a preconditioning operator. Results of a number of numerical examples show that by using this preconditioning operator, a large conductivity contrast of the unknown objects (factor of 100) can be reconstructed up to an acceptable degree of accuracy. Moreover, in each iteration, the computational effort to generate the preconditioning operator is negligible.

Index Terms—Cross-well, induction logging, nonlinear inversion, three-dimensional.

I. INTRODUCTION

INTEREST in cross-well tomography (imaging) of the earth electrical conductivity has increased because of improvements in field instrumentation, computing power, and method of interpretation. Cross-well electromagnetic logging is a technique to investigate the geological properties of the region between boreholes from the electromagnetic measurements made in these boreholes at one or more frequencies for a large combination of source and receiver locations.

During the last decade, a number of nonlinear inversion methods has been employed to map the conductivity distribution between boreholes. For low-frequency measurements, the so-called induction logging, Alumbaugh and Morrison [3] have developed a multifrequency imaging procedure for the reconstruction of two-dimensional (2-D) variations of conductivity excited by electric line sources. In their approach, the Green function was fixed for a certain background, while the unknown electric field was updated after each iteration. A slightly different class of iterative methods undertakes repeated modifications of the Green function after each iteration. This method is known as the distorted Born iterative method [4]. This method is also used in a 2-D single-well problem by Chew and Liu [5] and a 3-D cross-well problem by Newman [7]. Note that in this method, one has to solve a full forward problem in each iteration. Torres-Verdin and Habashy [10] use a nonlinear inversion technique known as the iterative extended Born approximation to probe the 2-D object with the conductivity

contrast. They have shown that with the same computational efficiency of the first-order Born approximation, the extended Born approximation enables one to solve a much wider class of 2-D inverse scattering problem.

Recently, we have developed an inversion method to reconstruct a three-dimensional (3-D) cross-well conductivity distribution from the dc-resistivity or electrode logging measurements [2]. This method is called the contrast source inversion (CSI) method, and has been originally introduced by van den Berg and Kleinman [13] to handle the 2-D wave problem. Unlike most nonlinear inversion methods, the CSI method does not require some artificial regularization techniques to deal with the problems of the nonuniqueness in inversion of data. It attempts to overcome this problem by recasting the problem as an optimization problem, in which it seeks not only the contrast sources (the product between the total fields and the conductivity contrasts) but also the conductivity contrasts itself to minimize a cost functional consisting of two terms. The first term is the defect in matching measured (actual or synthetic) field data with the field scattered by a body with particular conductivity, and the second being the error in satisfying the integral equations for the field produced in the body by each excitation. An alternating method of iteratively solving this optimization problem is proposed, in which first the contrast source is updated in the conjugate gradient direction weighted so as to minimize the cost functional, and then the conductivity contrast is updated to minimize the error in the object equation using the update contrast source. This latter minimization can be done analytically, which allows an easy implementation of the positivity constraint for the conductivity. In order to guarantee the error reducing nature of the algorithm, the CSI method has been improved (see van den Berg *et al.* [14]). In this extended version, the conductivity contrast is updated also in a conjugate gradient step to minimize the second term in the cost functional, the object error.

In the present paper, we have extended the CSI method to handle the full-vector complex 3-D cross-well induction logging problem. For the forward problem, the concept of the extended Born approximation has been used to arrive at a preconditioning operator for the conjugate gradient method. In the inverse problem, the cost functional of the CSI method has been modified to include the preconditioning operators as well. Numerical examples will show that these preconditioning operators allow us to handle a large contrast (a factor of 100). Moreover, because of the simple form of the preconditioning operators, the extra computational effort to obtain the preconditioning operator is negligible. Furthermore, it will also be shown that by using multi-components receivers the reconstruction results improve.

Manuscript received August 14, 1999; revised February 19, 2000.

The authors are with the Laboratory of Electromagnetic Research, Delft University of Technology, Delft, The Netherlands (e-mail: abubakar@its.tudelft.nl).
 Publisher Item Identifier S 0196-2892(00)05904-0.

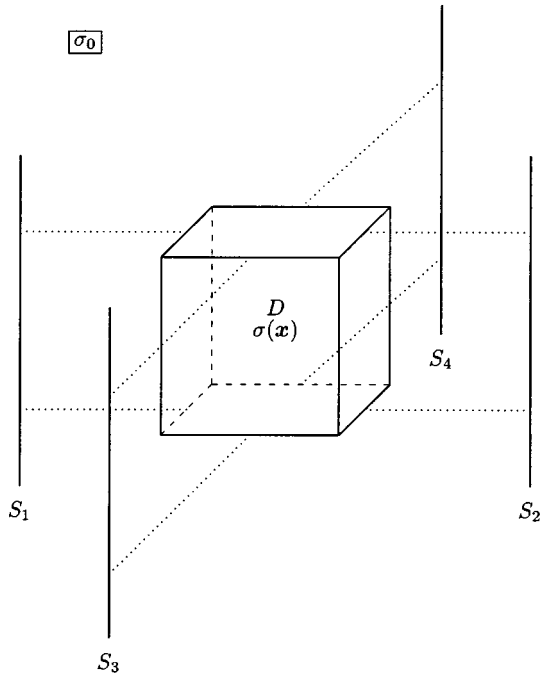


Fig. 1. Theoretical model of the cross-well configuration in the homogeneous background with conductivity σ_0 . The object domain D with conductivity $\sigma(\mathbf{x})$ is the domain to be reconstructed from the measurements made in the data domain $\{S_1, S_2, S_3, S_4\} \in S$.

II. INTEGRAL EQUATION FORMULATIONS

A theoretical model of the cross-well configuration is shown in Fig. 1. We define an inhomogeneous domain as an object domain D with conductivity $\sigma(\mathbf{x})$ embedded in an unbounded homogeneous background medium with conductivity σ_0 . The excitation source is a magnetic point dipole directed in the logging direction (vertical magnetic dipole) with a magnetic moment M^S located in the domain of S . This is a good approximation to the small transmitter coil used in induction tools. The measurement is also made in the domain of S . We measure either all the three components of the magnetic field or the vertical component of the magnetic field. The data domain S consists of four boreholes $\{S_1, S_2, S_3, S_4\} \in S$. In the present induction logging problem, we want to determine the conductivity distribution inside the object domain D from the measurements made in the data domain S .

Consider a Cartesian coordinate frame for which a given location \mathbf{x} is expressed in terms of the unit vectors \mathbf{i}_1 , \mathbf{i}_2 , and \mathbf{i}_3 in the x_1 , x_2 , and x_3 directions respectively (i.e. $\mathbf{x} = x_1\mathbf{i}_1 + x_2\mathbf{i}_2 + x_3\mathbf{i}_3$). We assume a time harmonic dependence $\exp(-i\omega t)$, where $i^2 = -1$, ω is angular frequency, and t is time. Maxwell's equations are given by

$$-\nabla \times \mathbf{H} + \sigma \mathbf{E} = \mathbf{0} \quad (1)$$

$$\nabla \times \mathbf{E} - i\omega\mu_0\mathbf{H} = -\mathbf{K}^{\text{ext}} \quad (2)$$

where μ_0 is the magnetic permeability in free space, and \mathbf{K}^{ext} is the impressed magnetic current source. Here, $\nabla = (\partial_1, \partial_2, \partial_3)$ denotes the spatial differentiation with respect to the position vector $\mathbf{x} = (x_1, x_2, x_3)$. In (1) and (2), all of the spatial vari-

ations in medium properties are contained in the conductivity distribution σ , given by

$$\sigma(\mathbf{x}) = \sigma'(\mathbf{x}) - i\omega\epsilon(\mathbf{x}) \quad (3)$$

where σ' is the ohmic conductivity, and ϵ is the dielectric permittivity. Note that due to the frequency range used by the induction tools, the second term in (3) can be neglected. Then, σ is real and positive.

To cast (1) and (2) in an integral form, the actual configuration (object domain D) in which the field must be computed or the conductivity contrast to be inverted is embedded into a medium for which the point source solution for $\mathbf{K}^{\text{ext};G} = \delta(\mathbf{x})\mathbf{I}$ can be determined analytically. The simplest medium in this category is the unbounded homogeneous medium with conductivity σ_0 , where the point source solutions are obtained as

$$\mathbf{E}^G(\mathbf{x}) = -\nabla \times G\mathbf{I}, \quad (4)$$

$$\mathbf{H}^G(\mathbf{x}) = -\left[\sigma_0 + \frac{1}{i\omega\mu_0}\nabla\nabla\cdot\right]G\mathbf{I} \quad (5)$$

where \mathbf{I} is a unit vector, and the scalar Green function $G = G(\mathbf{x})$ is given by

$$G(\mathbf{x}) = \frac{\exp[ik_0|\mathbf{x}|]}{4\pi|\mathbf{x}|} \quad (6)$$

in which

$$k_0 = (i\omega\mu_0\sigma_0)^{\frac{1}{2}}. \quad (7)$$

We define \mathbf{E}^P as the primary electric field measured in the background and excited by the impressed magnetic current source \mathbf{K}^{ext} . This field is represented as

$$\mathbf{E}^P(\mathbf{x}) = -\nabla \times \int_{\mathbf{x}' \in S} G(\mathbf{x} - \mathbf{x}')\mathbf{K}^{\text{ext}}(\mathbf{x}') d\mathbf{v}'. \quad (8)$$

Starting from (1)–(8) and using the superposition principle for the electric and magnetic fields

$$\mathbf{E} = \mathbf{E}^P + \mathbf{E}^s \quad \text{and} \quad \mathbf{H} = \mathbf{H}^P + \mathbf{H}^s \quad (9)$$

where \mathbf{E}^s and \mathbf{H}^s are the secondary fields, we arrive at

$$\mathbf{E}^P(\mathbf{x}) = \mathbf{E}(\mathbf{x}) - [k_0^2 + \nabla\nabla\cdot]\mathbf{A}(\mathbf{x}), \quad \mathbf{x} \in D. \quad (10)$$

The normalized vector potential \mathbf{A} is given by

$$\mathbf{A}(\mathbf{x}) = \int_{\mathbf{x}' \in D} G(\mathbf{x} - \mathbf{x}')\chi(\mathbf{x}')\mathbf{E}(\mathbf{x}') d\mathbf{v}'. \quad (11)$$

In (11), we have introduced a conductivity contrast χ as

$$\chi(\mathbf{x}) = \frac{\sigma(\mathbf{x}) - \sigma_0}{\sigma_0}. \quad (12)$$

Equation (10) is the well-known integral equation to develop an imaging procedure for low-frequency electromagnetic measurements [10], [11], [16].

In the induction logging problem, we are interested in the secondary magnetic field \mathbf{H}^s . This secondary magnetic field \mathbf{H}^s can also be represented in term of an integral equation

$$\mathbf{H}^s(\mathbf{x}^R) = \sigma_0\nabla^R \times \mathbf{A}(\mathbf{x}^R), \quad \mathbf{x}^R \in S. \quad (13)$$

We observe that (10) is a singular integral equation in which the grad-div ($\nabla\nabla\cdot$) operator acts on a normalized vector potential \mathbf{A} , defined as the spatial convolutions of the Green function G and the product of the conductivity contrast χ and the total electric field \mathbf{E} . Numerical implementation of such an integral equation must be carried out carefully. We follow the discretization procedure of our previous work on the inversion of the electrode logging measurements [2]. In order to handle the singularity of the integral equation in (10), the normalized vector potential \mathbf{A} is replaced by its weak form (spherical mean). After that, the grad-div operator can be computed with the finite difference rule (see Abramowitz and Stegun [1]). This technique to cope with the singularity of the Green function has also been used by Richmond [9] to handle the 2-D scattering problem. Note that the normalized vector potential \mathbf{A} consists of spatial convolutions and can efficiently be computed by fast Fourier transform (FFT) routines (Press *et al.* [8]).

III. FORWARD SCATTERING PROBLEM

When the conductivity contrast χ is known, the discretized forward scattering problem for each excitation may be formulated as a linear system of equations. This linear system of equations can be written compactly in an operator notation as follows:

$$\mathbf{E}^{p,(i)} = \mathbf{E}^{(i)} - \mathcal{K}_D \chi \mathbf{E}^{(i)}, \quad \text{on } D \quad (14)$$

where the operator expression $\mathcal{K}_D \chi \mathbf{E}^{(i)}$ is directly obtained from the second term of the right-hand side of (10), and the superscript (i) denotes the numbering of the sources. Equation (14) is also called the object equation that holds on the object domain D . Since the matrix operator \mathcal{K}_D consists of spatial convolutions, we can use advantageously FFT routines (Zwamborn and van den Berg [17]). However, we then need an iterative solution, and the conjugate gradient (CG) method seems to be one of the most efficient methods. With this so-called CGFFT technique we are able to solve complex 3-D problems efficiently. Furthermore, it also gives the fundament of our solution for the inverse problem.

A. Forward Algorithm

The CG method consists of an algorithm to construct sequences of electric field $\mathbf{E}^{(i)}$ in D which iteratively reduce the value of the cost functional

$$\mathcal{F}_D = \frac{\sum_i \|\mathbf{E}^{p,(i)} - \mathbf{E}^{(i)} + \mathcal{K}_D \chi \mathbf{E}^{(i)}\|_D^2}{\sum_i \|\mathbf{E}^{p,(i)}\|_D^2} \quad (15)$$

where the norm on D is defined as

$$\|\mathbf{E}^{(i)}\|_D^2 = \int_{\mathbf{x}' \in D} \mathbf{E}^{(i)}(\mathbf{x}') \cdot \bar{\mathbf{E}}^{(i)}(\mathbf{x}') dv' \quad (16)$$

in which the overbar denotes the complex conjugate.

We construct sequences $\{\mathbf{E}_k^{(i)}\}$, for $k = 1, 2, \dots$, in the following manner. Define the object error in D to be

$$\mathbf{r}_k^{(i)} = \mathbf{E}^{p,(i)} - \mathbf{E}_k^{(i)} + \mathcal{K}_D \chi \mathbf{E}_k^{(i)}. \quad (17)$$

We update the total electric field $\mathbf{E}^{(i)}$ as follows:

$$\mathbf{E}_0^{(i)} = \mathbf{0}, \quad \mathbf{E}_k^{(i)} = \mathbf{E}_{k-1}^{(i)} + \alpha_k^{(i)} \mathbf{e}_k^{(i)}, \quad k \geq 1 \quad (18)$$

where $\alpha_k^{(i)}$ is constant and the update directions $\mathbf{e}_k^{(i)}$ are functions of position. The update directions are chosen to be the Fletcher-Reeves gradient directions

$$\mathbf{e}_0^{(i)} = \mathbf{0}, \quad \mathbf{e}_k^{(i)} = \partial \mathbf{e}_k^{(i)} + \frac{\|\partial \mathbf{e}_k^{(i)}\|_D^2}{\|\partial \mathbf{e}_{k-1}^{(i)}\|_D^2} \mathbf{e}_{k-1}^{(i)}, \quad k \geq 1. \quad (19)$$

Here $\partial \mathbf{e}_k^{(i)}$ is the preconditioned gradient of the cost functional \mathcal{F}_D with respect to $\mathbf{E}^{(i)}$ evaluated at $\mathbf{E}_{k-1}^{(i)}$. Explicitly this is found to be

$$\partial \mathbf{e}_k^{(i)} = \frac{\mathcal{P}_D \mathcal{P}_D^* (\mathbf{r}_{k-1}^{(i)} - \bar{\chi} \mathcal{K}_D^* \mathbf{r}_{k-1}^{(i)})}{\sum_i \|\mathbf{E}^{p,(i)}\|_D^2} \quad (20)$$

where \mathcal{K}_D^* is the adjoint of \mathcal{K}_D mapping $L_2(D)$ into $L_2(D)$. Note that in view of the orthogonality of the gradients of the linear forward problem, in this case $\partial \mathbf{e}^{(i)}$, Fletcher-Reeves directions are identical with the Polak-Ribière directions, see Kleinman and van den Berg [6]. As preconditioning operator \mathcal{P}_D we propose

$$\mathcal{P}_D(\mathbf{x}) = [\mathcal{I} - \chi \mathcal{K}_D \mathcal{I}]^{-1}(\mathbf{x}) \quad (21)$$

where \mathcal{I} is unit operator, and \mathcal{P}_D^* is the conjugate transpose of \mathcal{P}_D . The right-hand side of (21) represents a three by three matrix which is easily inverted for each \mathbf{x} .

This preconditioning operator \mathcal{P}_D is the approximate inverse of (14) using the extended Born approximation, introduced by Torres-Verdin and Habashy [10], [11]. However, we have brought the contrast source (the product of the conductivity contrast and total electric field) outside the integral operator instead of only the total electric field as Torres-Verdin and Habashy did. Numerical experiments indicate that the present version of the extended Born approximation works better as a preconditioning operator than the one introduced by Torres-Verdin and Habashy [10]. Furthermore, in the inverse problem the present version of the preconditioner is substantially less computer intensive, because the operator $\mathcal{K}_D \mathcal{I}$ does not change during the optimization process. The explicit expression of the preconditioning operator \mathcal{P}_D can be found in Appendix A.

After the update direction has been determined, the constant $\alpha_k^{(i)}$ is determined to minimize the cost functional in (15) rewritten as

$$\mathcal{F}_{D;k} = \frac{\sum_i \|\mathbf{r}_{k-1}^{(i)} - \alpha_k^{(i)} (\mathbf{e}_k^{(i)} - \mathcal{K}_D \chi \mathbf{e}_k^{(i)})\|_D^2}{\sum_i \|\mathbf{E}^{p,(i)}\|_D^2}. \quad (22)$$

The constant $\alpha_k^{(i)}$ is found explicitly to be

$$\alpha_k^{(i)} = \frac{\langle \mathbf{r}_{k-1}^{(i)}, \mathbf{e}_k^{(i)} - \mathcal{K}_D \chi \mathbf{e}_k^{(i)} \rangle_D}{\|\mathbf{e}_k^{(i)} - \mathcal{K}_D \chi \mathbf{e}_k^{(i)}\|_D^2}. \quad (23)$$

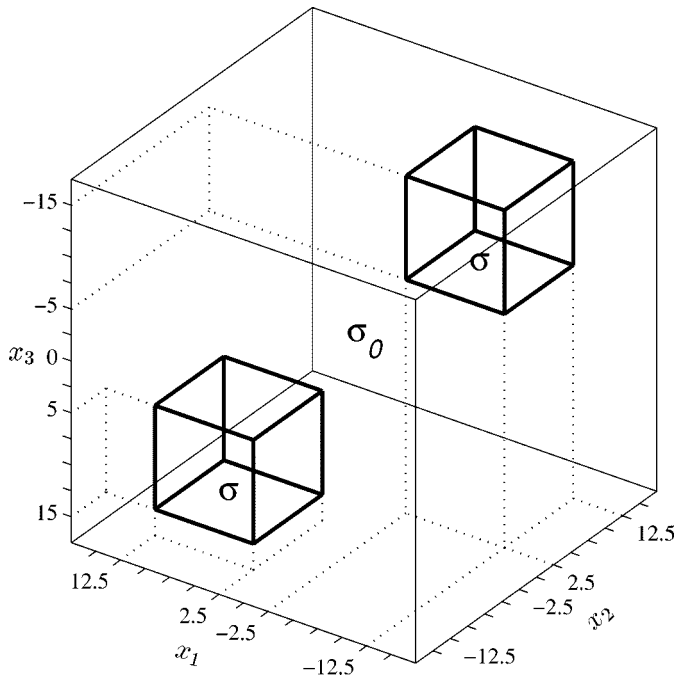


Fig. 2. Configuration of the dual conductivity model in the computation domain D with conductivity $\sigma_0 = 0.1$ S/m. In this domain, D we have two blocks of $10 \times 10 \times 10$ m³ with conductivity σ S/m.

Once the root mean square of $\mathcal{F}_{D;k}$ in (22) is small enough, the approximate solution of $\mathbf{E}_k^{(i)}$ is substituted in (13) to arrive at the secondary magnetic field $\mathbf{H}^{s;(i)}$ at the receiver position \mathbf{x}^R

$$\mathbf{H}^{s;(i)} = \mathcal{K}_S \chi \mathbf{E}^{(i)}, \quad \text{on } S \quad (24)$$

where

$$\begin{aligned} [\mathcal{K}_S \chi \mathbf{E}^{(i)}](\mathbf{x}^R) &= \sigma_0 \int_{\mathbf{x}' \in D} \mathcal{G}^R(\mathbf{x}^R - \mathbf{x}') \\ &\quad \times \chi(\mathbf{x}') \mathbf{E}^{(i)}(\mathbf{x}') dv', \quad \mathbf{x}^R \in S \end{aligned} \quad (25)$$

in which the matrix operator \mathcal{G}^R is given in (60) of Appendix I. The results of (24) will be used as synthetic measured data to test our inversion procedure.

B. Numerical Example

The discrete form of the algorithm is obtained by assuming that the object domain D is a rectangular domain with boundaries along the x_1 , x_2 , and x_3 directions. We discretize the object domain D in a rectangular mesh. The mesh is uniformly spaced in the x_1 , x_2 , and x_3 direction with widths of Δx_1 , Δx_2 , and Δx_3 . In each rectangular subdomain, we assume the conductivity contrast χ to be constant. The operator $\mathcal{K}_D \chi \mathbf{E}^{(i)} = [k_0^2 + \nabla \nabla \cdot] \mathbf{A}$ is computed using the technique which has been used to compute the integral operator in cross-well electrode logging problem (Abubakar and Van den Berg [2]).

As an example, we consider the 3-D model shown in Fig. 2. A dual-block model with conductivity σ located in a background medium with conductivity $\sigma_0 = 0.1$ S/m. Each block has dimensions of $10 \times 10 \times 10$ m³. The $35 \times 35 \times 35$ m³ test domain is divided into $14 \times 14 \times 14$ subdomains of $2.5 \times 2.5 \times 2.5$ m³.

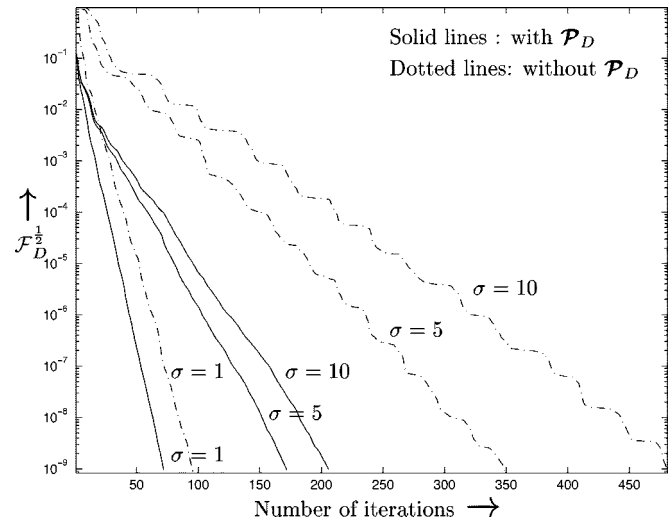


Fig. 3. Results of the conjugate gradient scheme using the concept of the extended Born approximation as the preconditioning operator (solid lines) and without using preconditioning operator (dashed lines).

Thus, the object domain is described by $-17.5 < x_1 < 17.5$, $-17.5 < x_2 < 17.5$, and $-17.5 < x_3 < 17.5$. Hence, the total number of the rectangular subdomains is equal to 2744.

For the cross-well induction logging problem, the vertical point magnetic dipole is a good approximation for the source modeling (Van der Horst *et al.* [15]). Using $\mathbf{K}^{\text{ext}} = i\omega\mu_0 M \delta(\mathbf{x} - \mathbf{x}^{S;(i)}) \mathbf{i}_3$ in (8), the primary electric field is given by

$$\begin{aligned} \mathbf{E}^{p;(i)}(\mathbf{x}) &= -i\omega\mu_0 M \frac{\exp(ik_0 |\mathbf{x} - \mathbf{x}^{S;(i)}|)}{4\pi |\mathbf{x} - \mathbf{x}^{S;(i)}|^3} \\ &\quad \times \left(ik_0 |\mathbf{x} - \mathbf{x}^{S;(i)}| - 1 \right) \\ &\quad \times \left[(x_2 - x_2^{S;(i)}) \mathbf{i}_1 - (x_1 - x_1^{S;(i)}) \mathbf{i}_2 \right] \end{aligned} \quad (26)$$

where M is the moment of the magnetic dipole. In this example, 24 point sources provides the source of excitations and are located in four boreholes (data domain S_1, S_2, S_3 , and S_4). These sources operate at a frequency of 20 kHz, and M is chosen to be unity.

In order to demonstrate the advantages of the use of the preconditioning operator \mathcal{P}_D in our forward algorithm, we plot the root mean square (RMS) of the cost-function $\mathcal{F}_D^{1/2}$ in (15) as a function of the number of iterations k (see Fig. 3). The solid lines denote the results of the conjugate gradient scheme using the preconditioning operator \mathcal{P}_D . The dashed lines denote the results of the nonpreconditioned scheme. By comparing these results, we observe that the preconditioned scheme is superior to the nonpreconditioned scheme. The superiority of the preconditioned scheme is very clear for the high contrast case ($\sigma = 10$). Note that the preconditioning operator \mathcal{P}_D for our forward scheme is only computed once, and it does not depend on the source excitation. Thus, in each iteration, the extra computational effort and the physical memory requirement of the use of the preconditioning operator \mathcal{P}_D are almost negligible. Obviously, we have constructed a very efficient preconditioner for the present cross-well induction logging problem.

IV. INVERSE SCATTERING PROBLEM

In the inverse problem, the secondary magnetic field $\mathbf{H}^{s,(i)}$ is measured at the measurement points \mathbf{x}^R . We assume that all the measurement points are located in the data domain S , outside D . The inverse induction logging problem is represented by (24). Equation (24) is denoted as the data equation that holds in the data domain S . The data equation contains both the unknown total electric field $\mathbf{E}^{(i)}$ and the unknown conductivity contrast χ , but they occur as a product that can be considered as a contrast source that produces the secondary magnetic field $\mathbf{H}^{s,(i)}$ at the measurement points. There is no unique solution for the contrast source by inverting the data equation by itself [13].

The CSI method attempts to overcome this difficulty by recasting the problem as an optimization, in which we seek not only the contrast sources but also the conductivity contrast itself to minimize a cost functional consisting of two terms, the L_2 errors in the data equation and in the object equation, rewritten in terms of the conductivity contrast and the contrast sources rather than the fields. An alternating method of iteratively solving this optimization problem is proposed, in which first the contrast sources are updated in the conjugate gradient step weighted so as to minimize the cost functional, and then the conductivity contrast is updated to minimize the object error using the updated contrast sources also with a conjugate gradient step. In this way, the error-reducing nature of the algorithm is enforced.

To this end, we introduce the contrast source $\mathbf{W}^{(i)}$ as follows:

$$\mathbf{W}^{(i)} = \chi \mathbf{E}^{(i)}. \quad (27)$$

The data equation becomes

$$\mathcal{K}_S \cdot \mathbf{W}^{(i)} = \mathbf{H}^{s,(i)}, \quad \text{on } S. \quad (28)$$

Substituting (14) into (27), we obtain an object equation for the contrast source $\mathbf{W}^{(i)}$ rather than for the field $\mathbf{E}^{(i)}$

$$\mathbf{W}^{(i)} - \chi \mathcal{K}_D \mathbf{W}^{(i)} = \chi \mathbf{E}^{p,(i)}, \quad \text{on } D. \quad (29)$$

Equation (29) is also called a source-type integral equation. The last two equations are the basic equations to develop the CSI method.

A. Inversion Algorithm

The CSI method consists of an algorithm to construct sequences of contrast sources $\mathbf{W}^{(i)}$ and sequences of conductivity contrasts χ in an alternating way that iteratively reduces the value of the cost functional

$$\mathcal{F} = \frac{\sum_i \|\mathcal{P}_S(\mathbf{H}^{s,(i)} - \mathcal{K}_S \mathbf{W}^{(i)})\|_S^2}{\sum_i \|\mathcal{P}_S \mathbf{H}^{s,(i)}\|_S^2} + \frac{\sum_i \|\mathcal{P}_D(\chi \mathbf{E}^{p,(i)} - \mathbf{W}^{(i)} + \chi \mathcal{K}_D \mathbf{W}^{(i)})\|_D^2}{\sum_i \|\mathcal{P}_D \chi \mathbf{E}^{p,(i)}\|_D^2} \quad (30)$$

where the norm on $L_2(D)$ is given by (16), and the norm on $L_2(S)$ is given by

$$\|\mathbf{H}^{(i)}\|_S^2 = \int_{\mathbf{x}^R \in S} \mathbf{H}^{(i)}(\mathbf{x}^R) \cdot \bar{\mathbf{H}}^{(i)}(\mathbf{x}^R) dV^R. \quad (31)$$

The normalizations are chosen such that both terms are equal to one if the contrast source $\mathbf{W}^{(i)}$ vanishes. The first term measures the error in the data equation, while the second term measures the error in the object equation. This is a quadratic functional in $\mathbf{W}^{(i)}$ but is highly nonlinear in χ . Note that in this cost functional, the object equation acts as a regularization for the data equation, and we have not employed other regularization techniques such as total variation, which has been proven effective for gradient-type methods [12].

Furthermore, the cost functional in (30) is different from the one used by Abubakar and van den Berg [2]. In the present paper, we have introduced two preconditioning operators, \mathcal{P}_S for the data equation and \mathcal{P}_D for the object equation. Here, we have used the preconditioning operators in the cost functional itself rather than only in the update directions as we did in the forward scattering problem (see (20)). This is due to present of the two different error terms in the cost functional which can not be preconditioned by the same preconditioning operator. The preconditioning operator $\mathcal{P}_S(\mathbf{x})$ is given by

$$\mathcal{P}_{S;\eta\kappa}(\mathbf{x}^R) = \frac{\mathcal{Q}_{\eta\kappa}}{|\mathcal{Q}_{\eta\kappa}|^{\frac{1}{2}}}, \quad \eta, \kappa \in \{1, 2, 3\} \quad (32)$$

where $\mathcal{Q}_{\eta\kappa}$ denotes the element of the matrix operator \mathcal{Q}

$$\mathcal{Q}(\mathbf{x}^R) = [\mathcal{K}_S \mathcal{K}_S^* \mathcal{I}]^{-1}(\mathbf{x}^R) \quad (33)$$

in which \mathcal{I} is a unit operator. Note that the preconditioning operator $\mathcal{P}_S(\mathbf{x})$ is the approximate inverse of the positive definite version of \mathcal{K}_S . The preconditioning operator \mathcal{P}_D is given in (21). More explicit expressions for \mathcal{Q} and \mathcal{P}_D can be found in Appendix I. Note that the preconditioning operator \mathcal{P}_S in (33) is only computed once during the iterative process. The preconditioning operator \mathcal{P}_D in (21) has to be computed in each iteration step because of the presence of the conductivity contrast χ , which is also updated during the optimization process. But the operator $\mathcal{K}_D \mathcal{I}$ is only computed once.

1) *Update of the Contrast Source $\mathbf{W}^{(i)}$* : The algorithm involves the construction of sequences $\{\mathbf{W}_k^{(i)}\}$ and $\{\chi_k\}$, $k \geq 1$ in the following manner. Define the data error and the object error at the k th step to be

$$\rho_k^{(i)} = \mathbf{H}^{s,(i)} - \mathcal{K}_S \mathbf{W}_k^{(i)} \quad \text{and} \quad \mathbf{r}_k^{(i)} = \chi_k \mathbf{E}_k^{(i)} - \mathbf{W}_k^{(i)} \quad (34)$$

where

$$\mathbf{E}_k^{(i)} = \mathbf{E}^{p,(i)} + \mathcal{K}_D \mathbf{W}_k^{(i)}. \quad (35)$$

Now suppose $\mathbf{W}_{k-1}^{(i)}$ and χ_{k-1} are known. We update $\mathbf{W}_k^{(i)}$ as follows:

$$\mathbf{W}_k^{(i)} = \mathbf{W}_{k-1}^{(i)} + \alpha_k^{(i)} \mathbf{w}_k^{(i)} \quad (36)$$

where $\alpha_k^{(i)}$ is spatially invariant, and $\mathbf{w}_k^{(i)}$ is the Polak-Ribière gradient direction

$$\begin{aligned} \mathbf{w}_0^{(i)} &= \mathbf{0}, \\ \mathbf{w}_k^{(i)} &= \partial \mathbf{W}_k^{(i)} + \frac{\langle \partial \mathbf{W}_k^{(i)}, \partial \mathbf{W}_k^{(i)} - \partial \mathbf{W}_{k-1}^{(i)} \rangle_D}{\|\partial \mathbf{W}_{k-1}^{(i)}\|_D^2} \mathbf{W}_{k-1}^{(i)}, \end{aligned} \quad \text{for } k \geq 1 \quad (37)$$

in which $\partial \mathbf{w}_k^{(i)}$ is the gradient (Fréchet derivative) of the cost functional \mathcal{F} in (30) with respect to $\mathbf{W}^{(i)}$ evaluated at $\mathbf{W}_{k-1}^{(i)}$ and χ_{k-1} . The motivation for the Polak-Ribière direction rather than the Fletcher-Reeves direction, as it has been chosen in the forward algorithm, is the presence of the conductivity contrast itself in the cost functional, which is also updated during the optimization process and hence disturbs the orthogonality properties of the gradients. Moreover, the Polak-Ribière direction is more robust when the difference of the succeeding gradients becomes small. The gradient $\partial \mathbf{w}_k^{(i)}$ is given by

$$\begin{aligned} \partial \mathbf{w}_k^{(i)} &= n_S \mathcal{K}_S^* \mathcal{P}_S^* \mathcal{P}_S \rho_{k-1} \\ &+ n_{D;k-1} \times (\mathcal{I} - \mathcal{K}_D^* \chi_{k-1}) \mathcal{P}_{D;k-1}^* \mathcal{P}_{D;k-1} \mathbf{r}_{k-1} \end{aligned} \quad (38)$$

where

$$\begin{aligned} n_S &= \left(\sum_i \left\| \mathcal{P}_S \mathbf{H}^{s;(i)} \right\|_S^2 \right)^{-1} \\ n_{D;k-1} &= \left(\sum_i \left\| \mathcal{P}_{D;k-1} \chi_{k-1} \mathbf{E}^{p;(i)} \right\|_D^2 \right)^{-1} \end{aligned} \quad (39)$$

and

$$\mathcal{P}_{D;k-1}(\mathbf{x}) = [\mathcal{I} - \chi_{k-1} \mathcal{K}_D]^{-1}(\mathbf{x}). \quad (40)$$

With the update directions completely specified, the coefficient $\alpha_k^{(i)}$ is determined to minimize the cost functional

$$\begin{aligned} \mathcal{F}_k &= n_S \sum_i \left\| \mathcal{P}_S \left(\rho_{k-1}^{(i)} - \alpha_k^{(i)} \mathcal{K}_S \mathbf{w}_k^{(i)} \right) \right\|_S^2 \\ &+ n_{D;k-1} \sum_i \left\| \mathcal{P}_{D;k-1} \left[\mathbf{r}_{k-1}^{(i)} \alpha_k^{(i)} \right. \right. \\ &\quad \left. \left. \times (\mathcal{I} - \chi_{k-1} \mathcal{K}_D) \mathbf{w}_k^{(i)} \right] \right\|_D^2 \end{aligned} \quad (41)$$

and found explicitly to be

$$\begin{aligned} \alpha_k^{(i)} &= \left(n_S \left\langle \mathcal{P}_S \rho_{k-1}^{(i)}, \mathcal{P}_S \mathcal{K}_S \mathbf{w}_k^{(i)} \right\rangle_S \right. \\ &+ n_{D;k-1} \left\langle \mathcal{P}_{D;k-1} \mathbf{r}_{k-1}^{(i)}, \mathcal{P}_{D;k-1} \right. \\ &\quad \left. \times (\mathcal{I} - \chi_{k-1} \mathcal{K}_D) \mathbf{w}_k^{(i)} \right\rangle_D \left. \right) \\ &\times \left(n_S \left\| \mathcal{P}_S \mathcal{K}_S \mathbf{w}_k^{(i)} \right\|_S^2 + n_{D;k-1} \left\| \mathcal{P}_{D;k-1} \right. \right. \\ &\quad \left. \left. \times (\mathcal{I} - \chi_{k-1} \mathcal{K}_D) \mathbf{w}_k^{(i)} \right\|_D^2 \right)^{-1}. \end{aligned} \quad (42)$$

Observe that we cannot start with $\mathbf{W}_0^{(i)} = \mathbf{0}$, since then $\chi = 0$, and the cost functional \mathcal{F}_k in (41) is undefined for iteration number $k = 1$. Therefore, we choose as starting values the values that minimize only the first term in (30), the data error

$$\mathbf{W}_0^{(i)} = \frac{\left\| \mathcal{K}_S^* \mathcal{P}_S^* \mathcal{P}_S \mathbf{H}^{s;(i)} \right\|_D^2}{\left\| \mathcal{K}_S \mathcal{K}_S^* \mathcal{P}_S^* \mathcal{P}_S \mathbf{H}^{s;(i)} \right\|_S^2} \mathcal{K}_S^* \mathcal{P}_S^* \mathcal{P}_S \mathbf{H}^{s;(i)}. \quad (43)$$

Note that $\mathcal{K}_S^* \mathcal{P}_S^* \mathcal{P}_S \mathbf{H}^{s;(i)}$ is the backpropagation of the data from the data domain S into the object domain D , and is often called a backpropagation of the field data.

Once the contrast source $\mathbf{W}_k^{(i)}$ is determined, the total electric field $\mathbf{E}_k^{(i)}$ in D is obtained by substituting the approximation of the contrast source $\mathbf{W}_k^{(i)}$ in (35), resulting in

$$\mathbf{E}_k^{(i)} = \mathbf{E}_{k-1}^{(i)} + \alpha_k^{(i)} \mathcal{K}_D \mathbf{w}_k^{(i)}. \quad (44)$$

2) *Update of the Conductivity Contrast χ* : The second step in the CSI method comprises the determination of the conductivity contrast χ in D . With the contrast source $\mathbf{W}_k^{(i)}$ and the total field $\mathbf{E}_k^{(i)}$, the conductivity contrast χ is updated as follows:

$$\chi_k = \chi_{k-1} + \beta_k \chi_k \quad (45)$$

where β_k is spatial invariant. The update direction χ_k is the Polak-Ribière gradient direction

$$\begin{aligned} \chi_0 &= 0, \\ \chi_k &= \partial \chi_k + \frac{\langle \partial \chi_k, \partial \chi_k - \partial \chi_{k-1} \rangle_D}{\left\| \partial \chi_{k-1} \right\|_D^2} \chi_{k-1}, \quad k \geq 1 \end{aligned} \quad (46)$$

where $\partial \chi_k$ is given by

$$\partial \chi_k = \frac{-\mathcal{P}_{D;k-1} \sum_i \left(\chi_{k-1} \mathbf{E}_k^{(i)} - \mathbf{W}_k^{(i)} \right) \cdot \overline{\mathcal{P}_{D;k-1} \mathbf{E}_k^{(i)}}}{\sum_i \left| \mathcal{P}_{D;k-1} \mathbf{E}_k^{(i)} \right|^2}. \quad (47)$$

Note that apart from the denominator, $\partial \chi_k$ is the gradient (Fréchet derivative) of the nominator of the second term of the cost functional in (30) with respect to χ evaluated at χ_{k-1} and $\mathbf{W}_k^{(i)}$.

With the update directions completely specified, the constant β_k is determined to minimize the second term of the cost functional in (30), rewritten as

$$\begin{aligned} \mathcal{F}_D &= \frac{\sum_i \left\| \mathcal{P}_{D;k-1} \left(\chi_k \mathbf{E}_k^{(i)} - \mathbf{W}_k^{(i)} \right) \right\|_D^2}{\sum_i \left\| \mathcal{P}_{D;k-1} \chi_k \mathbf{E}^{p;(i)} \right\|_D^2} \\ &= \frac{a \beta_k^2 + b \beta_k + c}{A \beta_k^2 + B \beta_k + C} \end{aligned} \quad (48)$$

where

$$\begin{aligned} a &= \sum_i \left\| \mathcal{P}_{D;k-1} \chi_k \mathbf{E}_k^{(i)} \right\|_D^2 \\ b &= \text{Re} \sum_i \left\langle \mathcal{P}_{D;k-1} \left(\chi_{k-1} \mathbf{E}_k^{(i)} - \mathbf{W}_k^{(i)} \right) \right. \\ &\quad \left. \mathcal{P}_{D;k-1} \chi_k \mathbf{E}_k^{(i)} \right\rangle_D \\ c &= \sum_i \left\| \mathcal{P}_{D;k-1} \left(\chi_{k-1} \mathbf{E}_k^{(i)} - \mathbf{W}_k^{(i)} \right) \right\|_D^2 \\ A &= \sum_i \left\| \mathcal{P}_{D;k-1} \chi_k \mathbf{E}^{p;(i)} \right\|_D^2 \\ B &= \text{Re} \sum_i \left\langle \mathcal{P}_{D;k-1} \chi_{k-1} \mathbf{E}^{p;(i)} \right. \\ &\quad \left. \mathcal{P}_{D;k-1} \chi_k \mathbf{E}^{p;(i)} \right\rangle_D \\ C &= \sum_i \left\| \mathcal{P}_{D;k-1} \chi_{k-1} \mathbf{E}^{p;(i)} \right\|_D^2. \end{aligned}$$

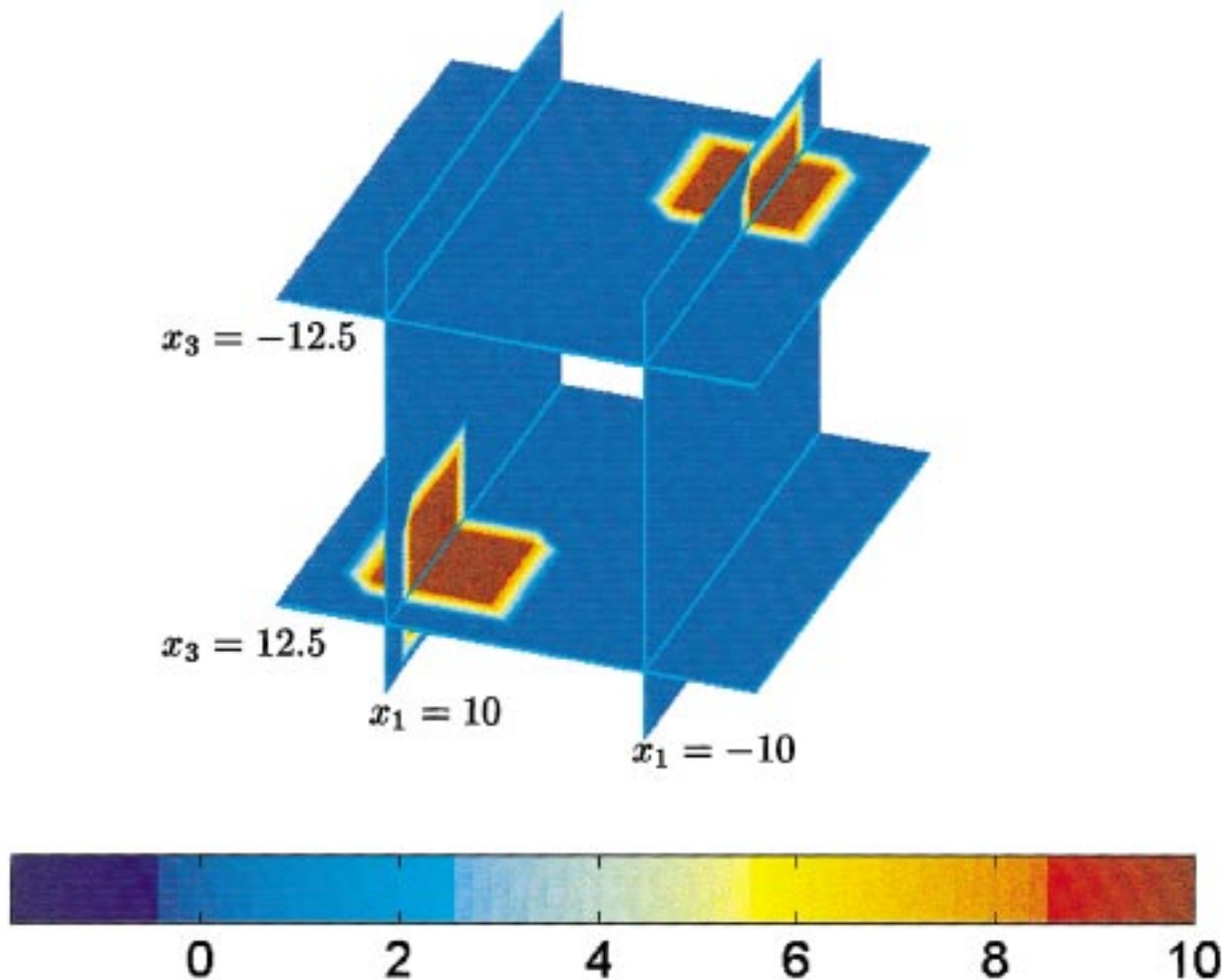


Fig. 4. Four slices of the 3-D conductivity distribution of the exact profile. These are slices of $x_1 = -10$, $x_1 = 10$, $x_3 = -12.5$ and $x_3 = 12.5$.

This is the quotient of two quadratics which, using elementary analysis, may be shown to attain its minimum when

$$\beta_k = \frac{-(aC - Ac)}{2(aB - Ab)} + \frac{\sqrt{(aC - Ac)^2 - 4(aB - Ab)(bC - Bc)}}{2(aB - Ab)}. \quad (49)$$

Unlike in [2] and [13], in this present CSI method, the error-reducing nature of the algorithm has been enforced.

Furthermore, in the present problem, we know that the conductivity σ is a positive quantity. The nonnegativity of the conductivity σ is incorporated into the algorithm by using

$$\zeta^2 = \frac{\sigma}{\sigma_0} = \chi + 1. \quad (50)$$

Instead of updating the conductivity contrast χ , we update ζ as

$$\zeta_k = \zeta_{k-1} + \beta_k \xi_k \quad (51)$$

with the direction ξ_k given by

$$\xi_0 = 0, \quad \xi_k = \partial \xi_k + \frac{\langle \partial \xi_k, \partial \xi_k - \partial \xi_{k-1} \rangle_D}{\|\partial \xi_{k-1}\|_D^2} \xi_{k-1}, \quad k \geq 1 \quad (52)$$

where

$$\partial \xi_k = 2\zeta_{k-1} \partial \chi_k \quad (53)$$

and $\partial \chi_k$ is given by (47). Note that the contrast gradient $\partial \xi_k$ vanishes for zero values of ζ_{k-1} . We therefore cannot start the iterative scheme with a zero estimate for ζ_0 . We use a backpropagation method to obtain a useful starting value for ζ_0 .

Furthermore, we note that at locations in the domain where ζ_{k-1} vanishes, there is no new gradient direction. This latter fact is responsible for the success of the reconstruction of an object. Now the constant β_k has to be determined by minimizing the functional in (48) for $\chi_k = \zeta_k^2 - 1$. These nonlinear equations are solved by using the Fletcher-Reeves-Polak-Ribière conjugate gradient method in [8]. This completes the description of the inversion algorithm.

B. Numerical Example

In order to demonstrate the advantage of using preconditioning operators \mathcal{P}_S and \mathcal{P}_D in our inverse scheme, we consider again the dual conductivity model described in Section III.B. In the configuration in Fig. 2, we have two objects with conductivity $\sigma = 10$ S/m. Note that in this example, we

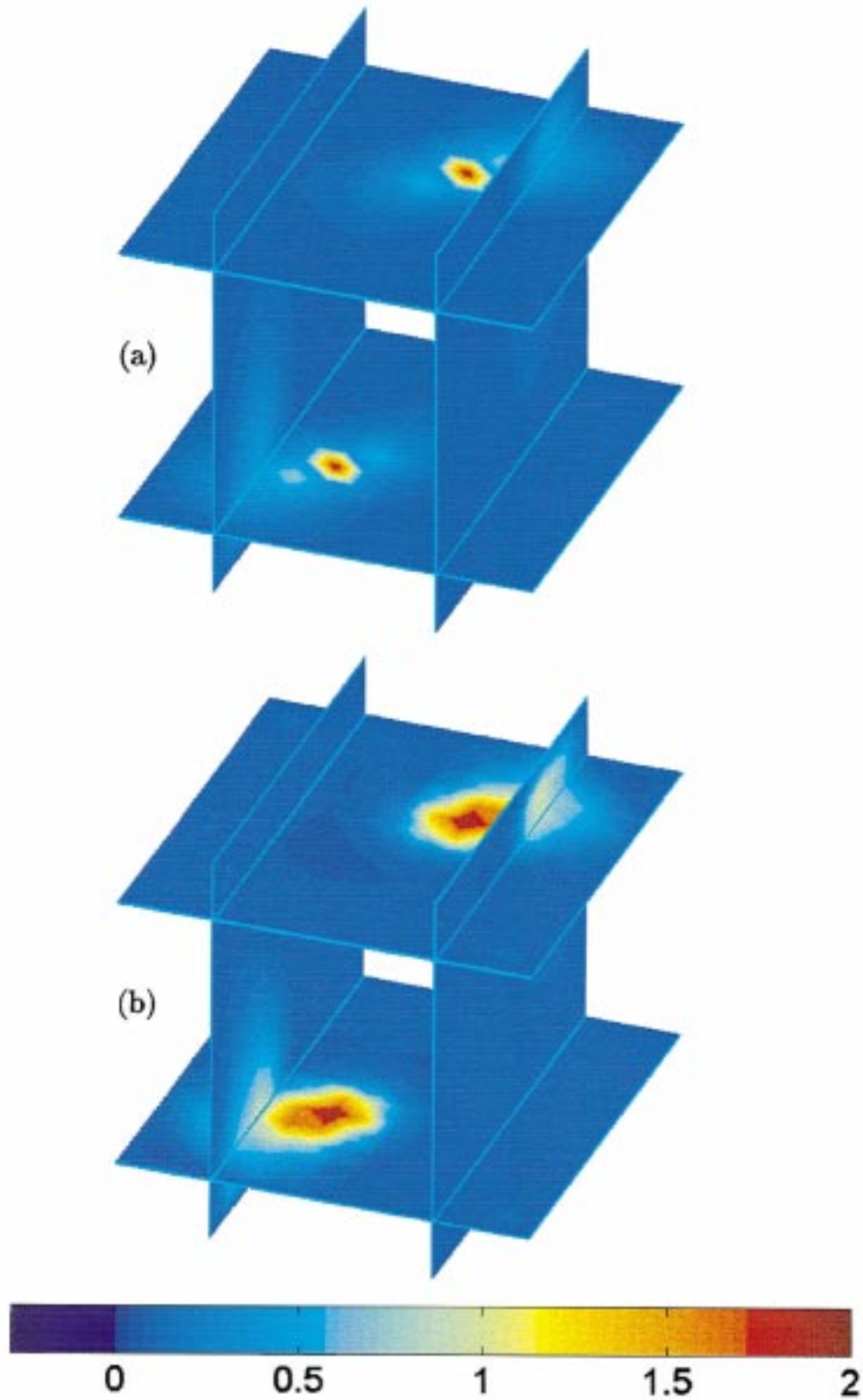


Fig. 5. Reconstructed 3-D conductivity distribution of (a) without and (b) with the preconditioning operators and using only the vertical component of the secondary magnetic field H_3^s .

have considered an extreme difficult case ($\chi = 99$) to demonstrate the performance of our approach. The conductivity of the background medium is $\sigma_0 = 0.1$ S/m. In the inversion

procedure, we assume that the unknown objects are located entirely within a test (object) domain with dimension $35 \times 35 \times 35$ m³, although knowledge of the precise location within

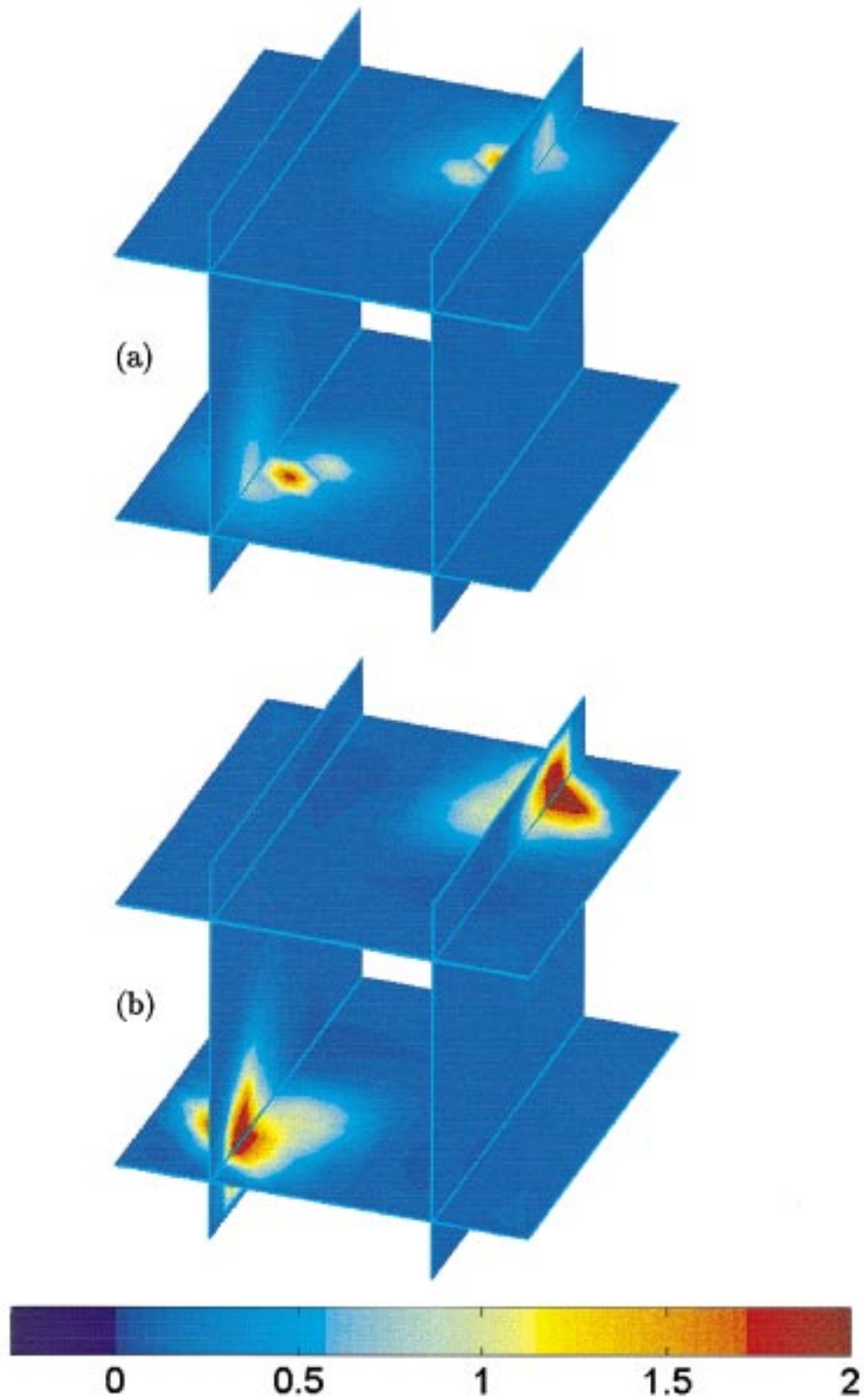


Fig. 6. Reconstructed 3-D conductivity distribution of (a) without and (b) with the preconditioning operators, using all three components of the secondary magnetic field H^s .

this test domain was not assumed. Thus, the object domain is described by $-17.5 < x_1 < 17.5$, $-17.5 < x_2 < 17.5$, and $-17.5 < x_3 < 17.5$. This test domain is divided into $14 \times$

14 subdomains with uniform side-length of 2.5 m. After discretization of the test domain D , the total number of the conductivity unknowns is equal to 2744.

In Fig. 4, we give four plane slices of the conductivity distribution $\sigma(\mathbf{x})$ of the configuration which has been used to generate the synthetic data using conjugate gradient method described in Section III.A but with a finer discretization grid. These are slices of $x_1 = -10$, $x_1 = 10$, $x_3 = -12.5$ and $x_3 = 12.5$. For the forward problem the test domain is subdivided into $28 \times 28 \times 28$ subdomains with uniform side-length of 1.25 m.

The synthetic data simulated at 20 kHz are generated using 24 point sources and 27 multicomponents receivers. Each source of excitation located on a particular borehole has 27 receivers located in the other three boreholes. Thus, in total we have 648 data points. In Fig. 5(a), we give the reconstruction results after 1024 iterations of the scheme without using preconditioning operators from single component data (the vertical component of the secondary magnetic field H_3^s). Although the total amount of the iteration is large, note that we do not solve a full forward problem in each iteration of the inversion procedure. One iteration of the inverse scheme takes approximately 27 s on a 400 MHz Pentium II personal computer.

In Fig. 5(b), we give the reconstruction results after 1024 iterations of the scheme using preconditioning operators also from single component data. Now, one iteration of this preconditioned scheme takes approximately 30 s. The same level of error in contrast of the nonpreconditioned scheme has been achieved by the preconditioned scheme only at iteration number $k = 201$. We observe the result in Fig. 5(b) is obviously better than the one in Fig. 5(a), and the preconditioned scheme does not increase the computation time significantly. In order to improve the reconstruction results, we use now all components of the secondary magnetic field \mathbf{H}^s instead of only its vertical component H_3^s as our known data in the inversion procedure. In Fig. 6(a), we give the reconstruction results after 1024 iterations of the scheme without using preconditioning operators and using all components of the secondary magnetic fields \mathbf{H}^s .

The results of the preconditioned scheme after 1024 iterations are given in Fig. 6(b). Now the maximum value of the reconstructed conductivity $\sigma_k^{\max} \simeq 2.41$. Indeed, once again we observe the superiority of the preconditioned scheme. Moreover, by comparing Figs. 5(a) and 6(a), and Figs. 5(b) and 6(b), we conclude that by using multi components data the general position of the targets (dual-block) are reconstructed more accurately. Note that although the value of the reconstructed conductivity is still not correct, the general position and dimensions of the dual-blocks conductivity is reconstructed very well. This smoothing and low value conductivity of the resulting image is due to the ill-posed nature of the problem and the very high conductivity to be reconstructed. We expect that the resolution of the images may improve as we learn more about the appropriate controls on the inversion parameters (adding an extra regularization term as in [14]).

Furthermore, in order to have more detailed information about the reconstructed profiles, we present in Fig. 7 three 1-D, the conductivity distributions as a function of vertical position x_3 for a fixed transverse positions of x_1 , and x_2 . The transverse positions are given by $(-11.25, 11.25)$, $(-8.75, 8.75)$, and $(-1.25, 1.25)$. The actual profiles are indicated by solid lines. The inversion results without using preconditioning

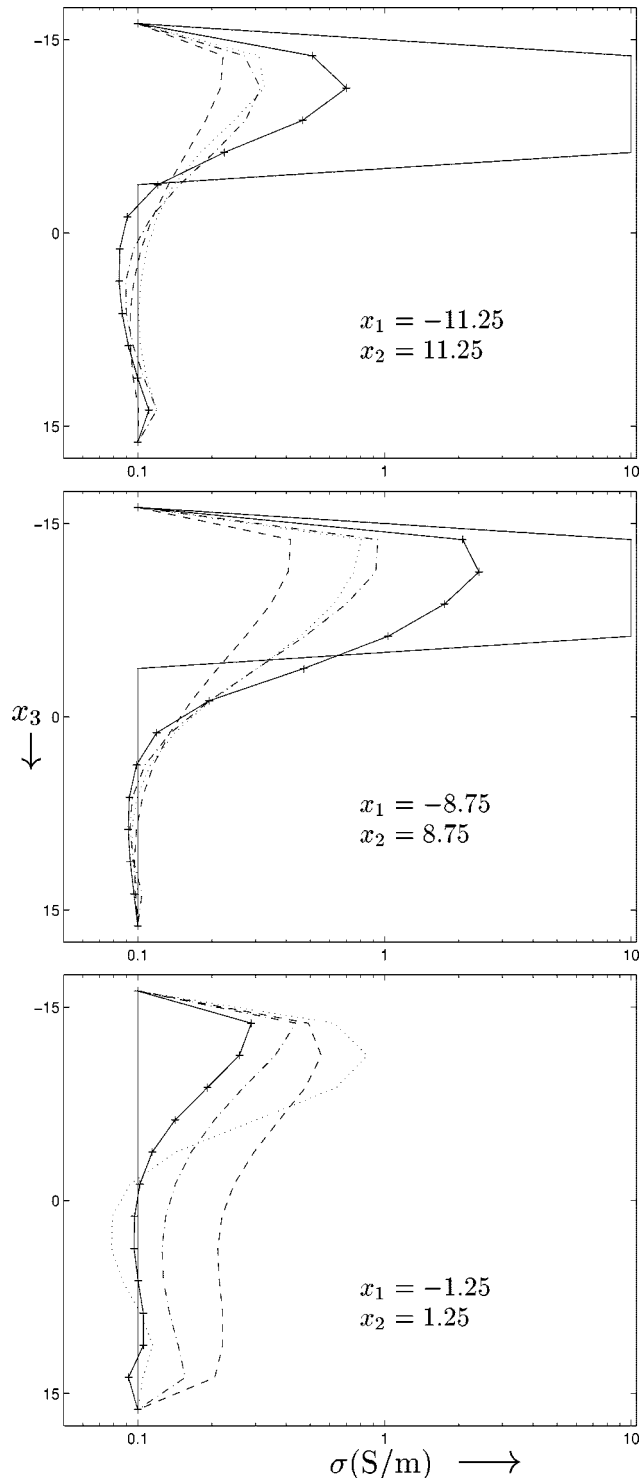


Fig. 7. Conductivity distribution of the exact profiles (solid-lines), and those of the reconstructed profiles (dashed-lines) without preconditioning operator using only H_3^R , dotted-lines with preconditioning operator using only H_3^R , dashed-dotted-lines without preconditioning operator using \mathbf{H}^R , solid-plus lines with preconditioning operator using \mathbf{H}^R .

operator are given by dashed-lines for the scheme using only single component data, and dashed-dotted lines for the scheme using multicomponents data. The reconstruction results using preconditioning operators are given by dotted-lines for the scheme using single component data, and solid-plus-lines for the scheme using all components of the magnetic field.

Note that the reconstruction results for fixed lateral positions $(-11.25, 11.25)$, $(-8.75, 8.75)$, and $(-1.25, 1.25)$ are identical.

From the last result, we observe that the present inversion method with preconditioning operators using multicomponents magnetic field data was successful in separating the two blocks and obtaining a relatively accurate description of their individual dimensions and their relative positions. Note that in this example, we have taken the most difficult case $\sigma = 10$ S/m. For the lower conductivity case $\sigma = 1$ S/m and $\sigma = 5$ S/m, we have also observed the same results. But, the advantage of the use of the preconditioning operators is more obvious for the high conductivity case.

V. CONCLUSION

In this paper, we have developed a method that can handle a 3-D problem for the cross-well induction logging measurements. For the forward problem, we have introduced a preconditioning operator to accelerate the convergence of the scheme. The preconditioning operator is obtained using the concept of the extended Born approximation. Numerical examples have shown that we have constructed a very efficient preconditioner for the present cross-well induction logging problem.

For the inverse problem, we have introduced a new version of the CSI method that can include the use of preconditioning operators and guarantee the error-reducing nature of the algorithm. The preconditioning operator is obtained again from the concept of the extended Born approximation. The numerical examples showed that in spite of the large size of the conductivity contrast (a factor of 100) and the limited amount of data, the present inversion method with simple preconditioning operators can still give a reasonably good result. Moreover, in view of the simplicity of the preconditioning operators used, the extra computation time of the use of these operators in our forward and inverse algorithms are negligible. Furthermore, we have also observed that the use of multicomponents data allows us to reconstruct a more accurate position and dimension of the unknown targets.

APPENDIX I PRECONDITIONING OPERATORS

The preconditioning operator for the object equation \mathcal{P}_D in (21) can be written explicitly as

$$\mathcal{P}_D(\mathbf{x}) = [\mathcal{I} - \chi(\mathbf{x})(k_0^2 \mathcal{I} + \nabla \nabla) \Lambda_D(\mathbf{x})]^{-1} \quad (54)$$

where \mathcal{I} is a identity operator, and the scalar Λ_D is given by

$$\Lambda_D(\mathbf{x}) = \int_{\mathbf{x}' \in D} G(\mathbf{x} - \mathbf{x}') dv' \quad (55)$$

in which the green function G is given in (6). We observe again that $\Lambda_D(\mathbf{x})$ on $\mathbf{x} \in D$ is a singular equation. One possible way to compute this preconditioning operator is to compute it analytically for each discretization domain as Torres-Verdin and Habashy [10], [11] did. However, for our purposes, there is no reason to use a preconditioning operator that is implemented more accurately than the integral operator used. Thus, we will handle \mathcal{P}_D with the same technique we have used to numerically implement the operator \mathcal{K}_D (see Abubakar and van den Berg [2]). The scalar function $\Lambda_D(\mathbf{x})$ is weakened by taking the spherical mean of it. We integrate $\Lambda_D(\mathbf{x})$ over a spherical domain with a center at (x_1, x_2, x_3) . The radius of this patch is taken to be $(1/2)\Delta x = c(1/2) \min(\Delta x_1, \Delta x_2, \Delta x_3)$. The results are divided by the volume of the spherical domain with radius $1/2\Delta x$. We then may write

$$\Lambda_D(\mathbf{x}) = \int_{\mathbf{x}' \in D} \mathcal{G}(\mathbf{x} - \mathbf{x}') dv' \quad (56)$$

where we have interchanged the order of integrations such that Note that for the limiting case $\Delta x \rightarrow 0$, the weak form of the Green function \mathcal{G} for $|\mathbf{x}| > (1/2)\Delta x$ tends toward the strong form of the Green function, G . In fact, \mathcal{G} is mean value of the Green function over a spherical domain with center at (x_1, x_2, x_3) . After this weakening procedure, we are now able to compute the integral over the domain D in (56) numerically using trapezoidal rule. Then, $\nabla \nabla \Lambda_D(\mathbf{x})$ is computed with the finite difference rule [1],[57], at the bottom of the next page].

An explicit expression for the preconditioning operator \mathcal{P}_D is finally written as

$$\mathcal{P}_D(\mathbf{x}) = \begin{bmatrix} l_{11}(\mathbf{x}) & l_{12}(\mathbf{x}) & l_{13}(\mathbf{x}) \\ l_{21}(\mathbf{x}) & l_{22}(\mathbf{x}) & l_{23}(\mathbf{x}) \\ l_{31}(\mathbf{x}) & l_{32}(\mathbf{x}) & l_{33}(\mathbf{x}) \end{bmatrix}^{-1} \quad (58)$$

where

$$\begin{aligned} l_{11}(\mathbf{x}) &= 1 - \chi(\mathbf{x})(k_0^2 + \partial_1^2) \Lambda(\mathbf{x}), \\ l_{12}(\mathbf{x}) &= l_{21}(\mathbf{x}) = -\chi(\mathbf{x})\partial_1 \partial_2 \Lambda(\mathbf{x}), \\ l_{13}(\mathbf{x}) &= -\chi(\mathbf{x})\partial_1 \partial_3 \Lambda(\mathbf{x}), \\ l_{22}(\mathbf{x}) &= 1 - \chi(\mathbf{x})(k_0^2 + \partial_2^2) \Lambda(\mathbf{x}), \\ l_{23}(\mathbf{x}) &= l_{32}(\mathbf{x}) = -\chi(\mathbf{x})\partial_2 \partial_3 \Lambda(\mathbf{x}), \\ l_{33}(\mathbf{x}) &= 1 - \chi(\mathbf{x})(k_0^2 + \partial_3^2) \Lambda(\mathbf{x}). \end{aligned}$$

$$\begin{aligned} \mathcal{G}(\mathbf{x}) &= \frac{6}{\pi(\Delta x)^3} \int_{|\mathbf{x}'| < \frac{1}{2}\Delta x} G(\mathbf{x} + \mathbf{x}') dv, \\ &= \begin{cases} \frac{[1 - \frac{1}{2}ik_0\Delta x] \exp(\frac{1}{2}ik_0\Delta x) - 1}{\frac{1}{6}\pi k_0^2 \Delta x^3}, & |\mathbf{x}| = 0, \\ \frac{\exp(ik_0|\mathbf{x}|) \left[\frac{\sinh(\frac{1}{2}ik_0\Delta x)}{\frac{1}{2}ik_0\Delta x} - \cosh(\frac{1}{2}ik_0\Delta x) \right]}{\frac{1}{3}\pi(k_0\Delta x)^2|\mathbf{x}|}, & |\mathbf{x}| > \frac{1}{2}\Delta x \end{cases} \end{aligned} \quad (57)$$

Note that for the present preconditioning operator, $\mathcal{P}_D(\mathbf{x})$ is a symmetric operator. The adjoint of the preconditioning operator $\mathcal{P}_D^*(\mathbf{x})$ is the complex conjugate of $\mathcal{P}_D(\mathbf{x})$.

The matrix operator $\mathcal{Q}(\mathbf{x}^R)$ in (33) can be written in more explicit terms as

$$\mathcal{Q}(\mathbf{x}^R) = \left[\sigma_0 \int_{\mathbf{x}' \in D} \mathcal{G}^R(\mathbf{x}^R - \mathbf{x}') \times \left(\sigma_0 \int_{\mathbf{x}' \in S} \mathcal{G}^{R*}(\mathbf{x}' - \mathbf{x}') dv' \right) dv \right]^{-1} \quad (59)$$

where

$$\mathcal{G}^R(\mathbf{x}^R - \mathbf{x}') = \begin{bmatrix} 0 & -\partial_3^R & \partial_2^R \\ \partial_3^R & 0 & -\partial_1^R \\ -\partial_2^R & \partial_1^R & 0 \end{bmatrix} G(\mathbf{x}^R - \mathbf{x}') \quad (60)$$

in which ∂_1^R , ∂_2^R , and ∂_3^R denote the spatial differentiations with regard to x_1^R , x_2^R , and x_3^R , respectively.

Unlike the operator $\mathcal{P}_D(\mathbf{x})$ on D , the $\mathcal{Q}(\mathbf{x}^R)$ on S can be implemented directly ($\mathbf{x}^R \neq \mathbf{x}$). An explicit expression for the preconditioning operator \mathcal{Q} is finally written as

$$\mathcal{Q}(\mathbf{x}^R) = \begin{bmatrix} l_{11}(\mathbf{x}^R) & l_{12}(\mathbf{x}^R) & l_{13}(\mathbf{x}^R) \\ l_{21}(\mathbf{x}^R) & l_{22}(\mathbf{x}^R) & l_{23}(\mathbf{x}^R) \\ l_{31}(\mathbf{x}^R) & l_{32}(\mathbf{x}^R) & l_{33}(\mathbf{x}^R) \end{bmatrix}^{-1} \quad (61)$$

where

$$l_{\eta\eta}(\mathbf{x}^R) = \int_{\mathbf{x}' \in D} \partial_{\kappa}^R G(\mathbf{x}^R - \mathbf{x}') \Lambda_{\kappa}^S(\mathbf{x}') dv' + \int_{\mathbf{x}' \in D} \partial_{\xi}^R G(\mathbf{x}^R - \mathbf{x}') \Lambda_{\xi}^S(\mathbf{x}') dv',$$

with (η, κ, ξ) cyclic,

$$l_{\eta\kappa}(\mathbf{x}^R) = - \int_{\mathbf{x}' \in D} \partial_{\eta}^R G(\mathbf{x}^R - \mathbf{x}') \Lambda_{\kappa}^S(\mathbf{x}') dv'$$

with $\eta \neq \kappa$

with $(\eta, \kappa, \xi) \in \{1, 2, 3\}$, in which

$$\Lambda_{\kappa}^S(\mathbf{x}') = \int_{\mathbf{x}' \in S} \overline{\partial_{\kappa}^{R'}} G(\mathbf{x}' - \mathbf{x}') dv^R \quad (62)$$

where the overbar denotes the complex conjugate.

ACKNOWLEDGMENT

The authors would like to thank H. Blok from Delft University of Technology, Delft, The Netherlands, for his encouraging scientific discussions about the extended Born approximation.

REFERENCES

- [1] M. Abramowitz and I. A. Stegun, *Handbook of Mathematical Functions*. New York: Dover, 1970.

- [2] A. Abubakar and P. M. van den Berg, "Three dimensional nonlinear inversion in cross-well electrode logging," *Radio Sci.*, vol. 33, no. 4, pp. 989–1004, 1998.
- [3] D. L. Alumbaugh and H. F. Morrison, "Theoretical and practical considerations for crosswell electromagnetic tomography assuming a cylindrical geometry," *Geophysics*, vol. 60, pp. 846–870, 1995.
- [4] W. C. Chew and Y. M. Wang, "Reconstruction of 2-D permittivity distribution using the distorted born iterative method," *IEEE Trans. Med. Imag.*, vol. 9, pp. 218–225, 1990.
- [5] W. C. Chew and Q. H. Liu, "Inversion of induction tool measurements using the distorted-born iterative method and CG-FFHT," *IEEE Trans. Geosci. Remote Sensing*, vol. 32, pp. 878–884, July 1994.
- [6] R. E. Kleinman and P. M. van den Berg, "Iterative methods for solving integral equations," in *Application of Conjugate Gradient Method to Electromagnetic and Signal Analysis PIER 5*, T. K. Sarkar, Ed. New York: Elsevier, 1991, pp. 67–102.
- [7] G. Newman, "Crosswell electromagnetic inversion using integral and differential equations," *Geophysics*, vol. 60, pp. 899–911, 1995.
- [8] W. H. Press, S. A. Teukolsky, W. T. Vetterling, and B. P. Flannery, *Numerical Recipes in Fortran: The Art of Scientific Computing*. New York: Cambridge Univ. Press, 1992, pp. 490–525.
- [9] J. H. Richmond, "Scattering by a dielectric cylinder of arbitrary cross section shape," *IEEE Trans. Antennas Propagat.*, vol. 13, pp. 334–341, 1965.
- [10] C. Torres-Verdin and T. M. Habashy, "Rapid 2.5-dimensional forward modeling and inversion via a new nonlinear scattering approximation," *Radio Sci.*, vol. 29, pp. 1051–1079, 1994.
- [11] —, "A two-step linear inversion of two-dimensional electrical conductivity," *IEEE Trans. Antennas Propagat.*, vol. 43, pp. 405–415, 1995.
- [12] P. M. van den Berg and M. van der Horst, "Nonlinear inversion in induction logging using the modified gradient method," *Radio Sci.*, vol. 5, pp. 1355–1369, 1995.
- [13] P. M. van den Berg and R. E. Kleinman, "A contrast source inversion method," *Inv. Probl.*, vol. 13, pp. 1607–1620, 1997.
- [14] P. M. van den Berg, A. Broekhoven, and A. Abubakar, "An extended contrast source inversion method," to be published.
- [15] M. van der Horst, V. Druskin, and L. Knizhnerman, "Modeling the response of induction logging tools in 3D geometries with the spectral lanczos decomposition method," in *Three-Dimensional Electromagnetics*. New York: SEG, 1995, pp. 611–622.
- [16] Q. Zhou, A. Becker, and H. F. Morrison, "Audio-frequency electromagnetic tomography in 2-D," *Geophysics*, vol. 58, pp. 482–495, 1993.
- [17] A. P. M. Zwamborn and P. M. van den Berg, "Computation of electromagnetic fields inside strongly inhomogeneous objects by the weak-conjugate gradient FFT method," *J. Opt. Soc. Amer.*, vol. 11, pp. 1414–1421, 1994.



Aria Abubakar was born in Bandung, Indonesia, on August 21, 1974. He received the M.Sc. degree (cum laude) in electrical engineering from the Delft University of Technology, Delft, The Netherlands, in 1997, where he is currently pursuing the Ph.D. degree in technical sciences.

In 1996, he was a Research Student with Shell Research B.V., Rijswijk, The Netherlands. He was a Summer Intern with Schlumberger-Doll Research, Ridgefield, CT, in 1999. He is currently with the Laboratory of Electromagnetic Research, Delft

University of Technology.

Mr. Abubakar was the recipient of the Best Master's Thesis Award in electrical engineering given by the Universiteitfonds Delft.



Peter M. van den Berg was born in Rotterdam, The Netherlands, on November 11, 1943. He received the degree in electrical engineering from the Polytechnical School of Rotterdam, Rotterdam, The Netherlands, in 1964, and the B.Sc. and M.Sc. degrees in electrical engineering and the Ph.D. degree in technical sciences, all from the Delft University of Technology, Delft, The Netherlands, in 1966, 1968, and 1971, respectively.

From 1967 to 1968, he was as a Research Engineer with the Dutch Patent Office. Since 1968, he has been a member of the Scientific Staff of the Electromagnetic Research Group, Delft University of Technology. During these years, he carried out research and taught classes in the area of wave propagation and scattering problems. From 1973 to 1974, he was a Visiting Lecturer with the Department of Mathematics, University of Dundee, U.K., financed by an award from the Niels Stensen Stichting, The Netherlands. During a three-month period in 1980–1981, he was a Visiting Scientist with the Institute of Theoretical Physics, Goteborg, Sweden. He was appointed Professor at the Delft University of Technology in 1981. From 1988 to 1994, he also carried out research at the Center of Mathematics of Waves, University of Delaware, Newark. These visits were financed by a NATO award. During the summers of 1993–1995, he was a Visiting Scientist with Shell Research B. V., Rijswijk, The Netherlands. Since 1994, he has also been a Professor with the Delft Research School Centre of Technical Geoscience. Currently, his main research interests are the efficient computation of field problems using iterative techniques based on error minimization, the computation of fields in strongly inhomogeneous media, and the use of wave phenomena in seismic data processing. His major interest is in an efficient solution of the nonlinear inverse scattering problem.